Joint Doppler and Azimuth DOA Tracking for Positioning with Iridium LEO Satellites

Shaghayegh Shahcheraghi, Forough Nasihati Gourabi, Mohammad Neinavaie, and Zaher M. Kassas
The Ohio State University

BIOGRAPHY

Shaghayegh Shahcheraghi is a Ph.D. student at The Ohio State University and member of the Autonomous Systems Perception, Intelligence, and Navigation (ASPIN) Laboratory. She received a B.E. in Electrical Engineering and an M.S. in Telecommunication engineering from Shiraz University. She obtained her second M.S. degree in Telecommunication engineering with the focus on signal processing from Polytechnic University of Milan, Italy. Her research interests include opportunistic navigation, blind opportunistic navigation, cognitive radio, wireless communication systems, and software-defined radio.

Forough Nasihati Gourabi is a postdoctoral scholar at The Ohio State University and a member of the Autonomous Systems Perception, Intelligence, and Navigation (ASPIN) Laboratory. She received a Ph.D. in Aerospace Engineering from the Sharif University of Technology. Her research interests include optimal estimation, opportunistic navigation, and satellite orbit determination.

Mohammad Neinavaie is a Ph.D. student at The Ohio State University and member of the Autonomous Systems Perception, Intelligence, and Navigation (ASPIN) Laboratory. He received a B.E. in electrical engineering and an M.S. in digital communication systems from Shiraz University. His research interests include opportunistic navigation, blind opportunistic navigation, cognitive radio, wireless communication systems and software-defined radio.

Zaher (Zak) M. Kassas is a professor at The Ohio State University and TRC Endowed Chair in Intelligent Transportation Systems. He is the Director of the Autonomous Systems Perception, Intelligence, and Navigation (ASPIN) Laboratory. He is also director of the U.S. Department of Transportation Center: CARMEN (Center for Automated Vehicle Research with Multimodal AssurEd Navigation), focusing on navigation resiliency and security of highly automated transportation systems. He received a B.E. in Electrical Engineering from the Lebanese American University, an M.S. in Electrical and Computer Engineering from The Ohio State University, and an M.S.E. in Aerospace Engineering and a Ph.D. in Electrical and Computer Engineering from The University of Texas at Austin. He is a recipient of the National Science Foundation (NSF) CAREER award, Office of Naval Research (ONR) Young Investigator Program (YIP) award, Air Force Office of Scientific Research (AFOSR) YIP award, IEEE Walter Fried Award, Institute of Navigation (ION) Samuel Burka Award, and ION Col. Thomas Thurlow Award. He is an Associate Editor of the IEEE Transactions on Aerospace and Electronic Systems and the IEEE Transactions on Intelligent Transportation Systems. He is a Fellow of the ION and a Distinguished Lecturer of the IEEE Aerospace and Electronic Systems Society. His research interests include cyber-physical systems, navigation systems, and intelligent transportation systems.

ABSTRACT

A receiver capable of estimating the Doppler and azimuth direction-of-arrival (DOA) of Iridium NEXT low Earth orbit (LEO) signals of opportunity (SOPs) is presented. The proposed receiver operates in three stages: (i) Fast Fourier Transform (FFT)-based Doppler acquisition, (ii) Kalman filter (KF)-based Doppler tracking, and (iii) Doppler-compensated MUltiple SIgnal Classification (MUSIC)-based algorithm for DOA tracking. Experimental results are presented demonstrating successful tracking of the Doppler frequency and azimuth DOA of an Iridium NEXT LEO satellite, achieving a Doppler root mean square error (RMSE) of 8.1 Hz over 120 seconds and an azimuth DOA RMSE of 1.04 degrees over 60 seconds. The Doppler and azimuth DOA measurements are fused via an extended Kalman filter (EKF) to localize a stationary receiver. Starting with an initial estimate 7 km away from the true receiver's position, the Doppler-only measurements yielded a final positioning error of 656.m, while the Doppler and azimuth DOA measurements reduced the error to 289.5 m.

I. INTRODUCTION

Over the past decade, the tremendous potential of signals of opportunity (SOPs) for navigation has been unveiled (Raquet *et al.*, 2021; Souli et al., 2021; Fokin and Volgushev, 2022; Kassas et al., 2022). SOPs include cellular (Wang and Morton, 2023; Liu et al., 2023; Tian et al., 2023; Kassas and Abdallah, 2023), FM radio (Moghtadaiee and Dempster, 2014; Aziz and Allen, 2018; Chen et al., 2020; Psiaki and Slosman, 2019), digital television (Yang and Soloviev, 2020; Hong et al., 2021; Souli et al., 2022; Jiao et al., 2023), low Earth orbit (LEO) satellites (Jardak and Jault, 2022; Huang et al., 2022; Zhao et al., 2023; Kassas et al., 2023a), and geostationary Earth orbit (GEO) satellites (Gao et al., 2021).

Among terrestrial SOPs, the most accurate navigation results have been demonstrated with cellular signals, achieving meter-level accuracy on ground vehicles (Soderini et al., 2020; Yang et al., 2022; Maaref and Kassas, 2022; Lapin et al., 2022) and sub-meter-level accuracy on unmanned aerial vehicles (UAVs) (Khalife and Kassas, 2023). Different techniques have been studied for cellular-based navigation. In (Shamaei et al., 2018; Shamaei and Kassas, 2021a), a long-term evolution (LTE) receiver was proposed, where the direction-of-arrival (DOA) and time-of-arrival (TOA) were jointly estimated, showing sub-meter-level positioning accuracy with 5 LTE eNodeBs. TOA estimates from real fifth generation (5G) signals showed meter-level ranging accuracy (Shamaei and Kassas, 2021b). Cramer-Rao lower bounds (CRLBs) of the direction-of-departure (DOD), DOA, and TOA for both uplink and downlink millimeter wave (mmWave) signals were derived in (Abu-Shaban et al., 2018), showing sub-meter positioning error, and sub-degree orientation error. To exploit the sparsity of mmWave channels, compressed sensing-based framework were proposed in (Lee et al., 2014) to estimate DOD, DOA, and TOA of the user equipment (UE), showing sub-meter-level position error via numerical simulation. The joint estimation of the position and orientation of the UE, as well as the location of reflectors or scatterers in the absence of the line-of-sightg (LOS) path were considered in (Mendrzik et al., 2018), showing less than 15 m position root-mean squared (RMSE) and less than 7 degrees orientation RMSE. The DOD and UE's position were estimated in a two-stage Kalman filter (KF) using the signal strength from multiple base stations in (Rastorgueva-Foi et al., 2018), which yielded sub-meter-level three-dimensional (3-D) position accuracy. In (Fascista et al., 2019), a positioning method for multiple-output single-input systems was proposed, where the DOD and TOA of the received signal were used to localize a UE. In (Ma et al., 2020), estimation of signal parameters via rotational invariant techniques (ESPRIT) was used to estimate the DOA and DOD of the signal.

LEO satellite SOPs have attracted considerable attention in recent years (Prol et al., 2022; Hartnett, 2022; Shi et al., 2023), due to their desirable characteristics for navigation: (i) compared with global navigation satellite systems (GNSS) which reside in medium Earth orbit (MEO), LEO satellites are about twenty times closer to Earth, which could result in higher received signal power; (ii) there are thousands of satellites in LEO, and it is expected that tens of thousands more space vehicles (SVs) will be deployed into LEO in the upcoming decade, which could provide more coverage and availability compared with terrestrial SOPs; and (iii) LEO SVs are deployed in different orbits and transmit in a wide range of frequency bands, providing both spatial and spectral diversity.

The potential of LEO signals for navigation have been the subject of several recent studies (Leng et al., 2016; Wei et al., 2020; Psiaki, 2021). Orbcomm LEO satellite signals were exploited for stationary receiver positioning in (Khalife and Kassas, 2019) and UAV navigation in (Khalife et al., 2020; Kozhaya and Kassas, 2022). Iridium NEXT LEO satellites were exploited for stationary receiver positioning in (Tan et al., 2019a) and aerial vehicle navigation in (Benzerrouk et al., 2019). Orbcomm and Iridium NEXT LEO satellites were jointly exploited for stationary receiver positioning in (Farhangian and Landry, 2020; Orabi et al., 2021) and for ground and aerial vehicle navigation in (Farhangian et al., 2021). Starlink signals were first acquired, tracked, and exploited for stationary receiver positioning in (Khalife et al., 2022). Ground vehicle navigation with Starlink, Orbcomm, and Iridium NEXT was first demonstrated in (Kassas et al., 2021). OneWeb signals were first acquired and tracked in (Kozhaya et al., 2023) and were used alongside Starlink, Orcomm, and Iridium for stationary receiver positioning, while ground vehicle navigation with these four constellations was demonstrated in Kassas et al. (2023b).

Nevertheless, all the aforementioned work relied on either the Doppler frequency or the carrier phase for positioning and navigation. While DOA estimation for positioning with terrestrial SOPs has been the subject of many studies (Pan et al., 2022), DOA estimation from LEO SOPs has not received similar attention. In (Islam et al., 2021), Doppler and DOA estimation of satellites in the UHF and VHF bands were studied. Using an L-shaped antenna array, DOA was estimated using the interferometer and MUltiple SIgnal Classification (MUSIC) techniques. The developed DOA estimation method was implemented only for amplitude shift keying (ASK) modulated signals, and in the UHF and VHF bands. In (Thompson et al., 2021), by incorporating the DOA, a differenced Doppler positioning method was proposed to address the issue of lack of knowledge about the precise location of satellites. DOA was estimated at the stationary base and shared with the roving receiver to derive the geometry matrix to eliminate the need for information about SVs' states. The simulation results showed that the DOA measurements should be very accurate to enable acceptable position estimation in case only a single LEO satellite is used. This work did not study how to estimate DOA of LEO SVs. In this paper, a Doppler compensated-aided MUSIC framework is proposed to track the azimuth DOA of the signals coming from Iridium NEXT satellites. To the authors' knowledge, this is the first study to consider joint Doppler and azimuth DOA tracking of Iridium NEXT LEO satellite SOPs for positioning.

Iridium NEXT LEO signals consist of multiple channels, namely, the ring alart (RA), paging channel, voice channel, and duplex user channels, which are transmitted over the 1,616–1,626.5 MHz band to provide different communication services globally. A small part of this spectrum, namely 1,626–1,626.5 MHz is used for paging and acquisition (Iridium Constellation LLC, 2013). In this paper, by setting the receiver frequency to 1,626.2708 MHz in the L–band, signals are collected from the RA channel of Iridium NEXT satellites to estimate the Doppler frequency. The RA channel bandwidth is B = 41.667 kHz. The Iridium NEXT constellation consists of 75 active satellites that orbit the Earth in 6 different orbital planes, spaced 30° apart (Iridium Constellation LLC, 2013).

The IRIDIUM NEXT signal employs both time division multiple access (TDMA) and frequency division multiple access

(FDMA) and consists of three parts, namely tone (no modulation), unique word (Binary Phase Shift Keying (BPSK) modulation) and information (Quadrature Phase Shift Keying (QPSK) modulation). In this paper, pure tone, BPSK and QPSK signals are exploited simultaneously for Doppler tracking of Iridium NEXT signals, enabling more precise Doppler estimation (Tan et al., 2019b) compared with tracking only the pure tone part of the signal. In addition to estimating the Doppler frequency, the paper also presents an approach for azimuth DOA estimation with a Uniform Linear Array (ULA).

This paper's contributions are as follows. First, a receiver architecture that could produce Doppler frequency and azimuth DOA observables from Iridium NEXT LEO satellites is presented. Second, the Doppler and azimuth DOA observables are fused via an extended Kalman filter (EKF) to localize a stationary receiver with a single Iridium NEXT LEO satellite. Starting with an initial estimate 7 km away from the true receiver's position, the Doppler-only measurements yielded a final positioning error of 656.m, while Doppler and azimuth DOA measurements reduced the error to 289.5 m.

The rest of the paper is organized as follows. Section II describes the received baseband signal model. Section III presents the proposed receiver architecture. Section IV presents the experimental results for Doppler and Azimuth DOA tracking along with receiver positioning with these observables. Section V gives concluding remarks.

II. RECEIVED BASEBAND SIGNAL MODEL

At the receiver, a ULA with M antenna elements where all the antennas are separated by the same distance d is used to estimate the azimuth DOA of the Iridium downlink signal using the phase difference of the received signal at different antenna elements and different samples. A very small gap between the antenna elements reduces directivity, while large spacing introduces grating lobes resulting in ambiguity in DOA estimation. Therefore, the spacing between antenna elements is typically chosen to be equal to half the wavelength ($d = \frac{\lambda}{2}$), where $\lambda = \frac{c}{f_c}$ is the received signal wavelength, c is the speed-of-light, and f_c is the carrier frequency (Clerckx and Oestges, 2013). The baseband signal samples of Iridium NEXT SVs received by the mth antenna element can be written as

$$r_m[n] = \sum_{i=1}^{N} \gamma_{i,m}(\tau_n) a_i[n] e^{j2\pi f_{D_{i,m}}[n] T_s n} e^{j\frac{2\pi}{\lambda} d \cdot \sin(\phi_i[n])(m-1)} + w_m[n], \tag{1}$$

where $r_m[n]$ is the received signal by the mth antenna element at the nth time instant; N is the total number of Iridium NEXT satellites; $\gamma_{i,m}(\tau_n)$ is the complex channel gain between the mth antenna element and the ith Iridium NEXT space vehicle (SV); τ_n is the sample time expressed in the receiver time; $a_i[n]$ represents the transmitted symbol at the nth time instant drawn from an $M-$ary phase shift keying constellation, i.e., $a = e^{j\frac{2\pi q}{M}}$ for $q \in \{0, \cdots, M-1\}$; $\phi_i[n]$ is the angle between the beam arriving from ith Iridium NEXT satellite and the orthogonal line to the ULA at the nth time instant; $f_{D_{i,m}}[n]$ is the instantaneous Doppler frequency at the mth antenna element at the nth time instant, T_s is the sampling time; and $w_m[n]$ captures the effect of noise and transmitted data at the mth antenna element, which is modeled as a complex zero-mean independent and identically distributed noise with variance σ_w^2. Processing the received signal is performed in some processing intervals, named as coherent processing intervals (CPIs). Small CPIs cannot capture enough power to enable signal processing and precise estimation. On the other hand, due to the high dynamics of the channel between the SVs and the receiver, the instantaneous Doppler frequency varies during large CPI. It is observed that for Iridium NEXT LEO SVs, a CPI large enough to yield acceptable performance is one resulting in the instantaneous Doppler frequency $f_{D_i}[n]$ being modeled as a linear function of time. In particular, $f_{D_i}[n]$ at the kth CPI can be modeled as

$$f_{D_i}[n] = f_{D_{k,i}} + \beta_{k,i} n T_s, \qquad k = 0, \cdots, K-1, \tag{2}$$

where $f_{D_{k,i}}$ is referred to as constant Doppler, $\beta_{k,i}$ is the Doppler rate at the kth processing interval corresponding to the ith Iridium NEXT satellite, and K is the total number of CPIs. During the defined CPI, the channel gain $\gamma_{i,m}(\tau_n)$, Doppler $f_{D_{k,i}}$, and the Doppler rate $\beta_{k,i}$ are all constant. Since channel gain is considered to be constant during one CPI, the channel gain can be denoted as the function of CPI index, i.e., $\gamma_{i,m}(\tau_n) = \gamma_{k,i,m}$. The received signal at the mth antenna element at nth time instant when the Doppler rate is wiped-off can be written as $r'_m[n] = \exp\big(-j\pi\beta_{k,i,m} n^2 T_s^2\big) r_m[n]$

$$r'_m[n] \quad = \sum_{i=1}^{N} \gamma_{k,i,m} a_i[n] e^{j2\pi f_{D_{k,i,m}} T_s n} e^{j\frac{2\pi}{\lambda} d.\sin(\phi_{k,i}[n])(m-1)} + w_{\mathrm{eq_m}}[n].$$

The next section discusses the receiver architecture for Doppler acquisition and Doppler and DOA tracking. For simplicity of notations the subscripts (i and m), which denote the ith Iridium NEXT SV and mth antenna element respectively, will be dropped in the sequel, unless it is required. Note that the Doppler estimation method is similar for all antenna elements.

III. RECEIVER ARCHITECTURE

This section overviews the proposed receiver architecture. The proposed receiver performs Doppler and DOA estimation in two sequential steps. In the first step, the Doppler frequency of each antenna element is estimated, and in the second step, the DOA is estimated. The Doppler frequency of each antenna element is estimated in two stages: (i) acquisition and (ii) tracking. Each of these stages is discussed in detail next.

1. Doppler Frequency Acquisition

As discussed in Section II, based on the selected CPI length herein, the instantaneous Doppler frequency is appropriately modeled as a linear function of time.

Iridium NEXT signals consist of three components (i) an un-modulated tone, (ii) a unique word with binary phase shift keying (BPSK) modulation, and (iii) information data with quadrature phase shift keying (QPSK) modulation that are always transmitted from Iridium NEXT SVs to the receiver (Shahriar, 2008). In order to avoid a phase shift arising from the unique word (BPSK) and the information data (QPSK), the baseband samples in each CPI are raised to the 4th power to wipe off the BPSK and QPSK symbols, resulting in a pure tone. As such, in addition to the pure tone that was exploited in (Orabi et al., 2021), unique word signals and information signals are also exploited for Doppler frequency estimation (Tan et al., 2019b). Then, a fast Fourier transform (FFT) of the signal of first and second CPI is taken, and the Doppler rate is calculated based on the shift in Doppler frequency during one CPI. Note that in the frequency-domain, the impulse-like peak occurs at the frequency which is equal to four times of the true Doppler frequency due to the fact that the signal samples were raised to the 4th power. As a result, the obtained Doppler rate and Doppler frequency should be normalized by four to get the appropriate estimates. After wiping off the normalized Doppler rate, an FFT of the 4th power of the samples in the first CPI is taken. The initial Doppler frequency is acquired by normalizing the frequency at which the impulse-like peak of FFT occurs.

2. KF-Based Doppler Frequency Tracking

After obtaining coarse estimates of the Doppler rate and Doppler frequency in the acquisition step, the receiver refines and maintains these estimates via a KF. Due to the SVs'high dynamics and the CPI length, employing a KF allows for improved Doppler estimation, since its formulation allows for arbitrary Doppler model order selection. The KF-based Doppler tracking algorithm is described next.

a) Doppler Dynamics Model

The time-varying component of the continuous-time true Doppler is a function of the true range rate between the LEO SV and the receiver and the time-varying difference between the receiver's and LEO SV's clock bias rate (i.e., drift). It assumed that the clock drift is constant, so it has a constant contribution to the Doppler. The discrete-time dynamic model of the Doppler state vector $\boldsymbol{x}_k = [f_{D_k}, \beta_k]^{\mathsf{T}}$ is given by

$$\boldsymbol{x}_{k+1} = \mathbf{F}\boldsymbol{x}_k + \mathbf{w}_k, \tag{3}$$

$$\mathbf{F} = \begin{bmatrix} 1 & T \\ 0 & 1 \end{bmatrix}, \qquad \mathbf{Q} = q_{\tilde{w}} \begin{bmatrix} \frac{T^3}{3} & \frac{T^2}{2} \\ \frac{T^2}{2} & T \end{bmatrix}, \tag{4}$$

where $\mathbf{F}$ is the discrete-time state transition matrix, $\mathbf{w}_k$ is a discrete-time process noise with zero-mean and covariance matrix $\mathbf{Q}$, $q_{\tilde{w}}$ is the power spectral density of the continuous-time-equivalent of the process noise driving the Doppler rate acceleration, and T is the time interval between two measurements, which is set to the CPI length.

b) KF-Based Doppler Tracking

Let $\hat{\boldsymbol{x}}_{k|l}$ denotes the KF estimate of $\boldsymbol{x}_k$ given all the measurements up to time-step $l \leqslant k$, and $\mathbf{P}_{k|l}$ denotes the corresponding estimation error covariance. Using the estimated Doppler and Doppler rate in the acquisition stage, $\hat{\mathbf{x}}_{0|0}$ and its corresponding $\mathbf{P}_{0|0}$ are estimated. The KF-based tracking algorithm follows the standard time-update procedure in KF. The KF measurement update is implemented based on the FFT estimate of the Doppler, which is discussed next. First, the Doppler rate wipe-off is performed as $r'_k[n] = \exp\big(-j2\pi\beta_k n^2\big) r_k[n]$, where n corresponds to all the samples in each CPI. Next, the following steps are performed sequentially: (i) the samples of each CPI are raised to the power 4, (ii) FFT is taken, (iii) the frequency at which the peak occurs is detected, and (iv) after normalizing this frequency by 4, $f_{D_{k+1}}$, which is used in calculating the innovation, is estimated. The proposed KF innovation is obtained as

$$\nu_{k+1} = f_{D_{k+1}} - \hat{f}_{D_{k+1|k}}, \tag{5}$$

which is a direct measure of the Doppler estimation error. Using the innovation and performing a measurement-update, the posterior Doppler state vector $\hat{\mathbf{x}}_{k|k}$ is estimated.

3. Doppler-Compensated-based MUSIC for DOA Tracking

The estimated Doppler frequency is wiped-off from the baseband received samples of each antenna element according to $\tilde{r}_m[n] \triangleq \exp\Big(-j2\pi \hat{f}_{D_m}[n]T_s n\Big) r_m[n]$. Hence, the received signal at the mth antenna element at nth time instant when the Doppler frequency is wiped-off can be written as

$$\tilde{r}_m[n] = \gamma_m(\tau_n) a[n] e^{j\zeta_m[n]} e^{j\frac{2\pi}{\lambda} d\sin(\phi[n])(m-1)} + \tilde{w}[n], \tag{6}$$

where $\zeta_m[n] = 2\pi(f_{D_m}[n] - \hat{f}_{D_m}[n])T_s n$, which represents the effect of the residual Doppler.
Collecting the Doppler compensated samples for all the antennas, an $M \times L$ matrix $\mathbf{Y}$ is formed, whose mth row includes L Doppler-compensated samples received by the mth antenna element. In order to estimate the DOA, the MUSIC algorithm is applied. MUSIC is a subspace-based super-resolution algorithm that relies on the eigenvalue decomposition of the sample covariance matrix of the received signal (Paulraj et al., 1993). Let, $\mathbf{R}_y = \frac{1}{L}\sum_{l=1}^{L} \boldsymbol{y}_l \boldsymbol{y}_l^{\mathsf{H}}$ be the sample covariance matrix of the received signal, where $\boldsymbol{y}_l$ denotes the lth column of $\mathbf{Y}$. The intuition behind MUSIC comes from the fact that given a sufficient received signal power, $\mathbf{R}_y$ can be decomposed into two almost orthogonal subspaces: a noise subspace and a signal subspace. The eigenvalues corresponding to the signal subspace will be significantly larger than the ones associated with the noise subspace. The eigenvectors associated with the near-zero eigenvalues of $\mathbf{R}_y$ span the noise subspace and constitute the columns of the noise matrix, $\mathbf{U}_n$. Finally, the angular MUSIC spectrum can be computed as $\mathrm{P}_{MUSIC}(\phi) = \frac{1}{\boldsymbol{a}^{\mathsf{H}}(\phi)\mathbf{U}_n\mathbf{U}_n^{\mathsf{H}}\boldsymbol{a}(\phi)}$ for different values of ϕ, when $\boldsymbol{a}^{\mathsf{T}}(\phi) = \Big[1, e^{j\frac{2\pi}{\lambda}d\sin(\phi)}, ..., e^{j\frac{2\pi}{\lambda}d\sin(\phi)(M-1)}\Big]$ is the steering vector associated with the azimuth angle ϕ. Whenever the steering vector is related to the true angle of the received signal, the noise subspace and the steering vector becomes almost orthogonal to each other, resulting in sharp peaks in the angular MUSIC spectrum. These peaks represent the DOA estimates of the received signals.

IV. EXPERIMENTAL RESULTS

This section presents experimental results of Doppler and azimuth DOA tracking of signals from an unknown Iridium NEXT LEO SV via the proposed framework. Also, the positioning accuracy of a stationary receiver is compared for two scenarios, (i) only Doppler is exploited for positioning, (ii) both Doppler and azimuth angle are used for positioning. In what follows, the experimental setup is first discussed. Next, results from the Doppler acquisition, Doppler tracking, and azimuth DOA tracking of the Iridium NEXT are presented. Finally, Doppler-only and Doppler+azimuth DOA positioning results are presented.

1. Experimental Setup

To demonstrate the performance of the proposed receiver, an experiment was performed in Columbus, Ohio, USA. A stationary receiver was equipped with

- A National Instrument (NI) four-channel universal software radio peripherals (USRPs)-2955 to simultaneously down-mix and synchronously sample the Iridium NEXT signals received by four antennas at a sampling rate of 2.4 Msps and a carrier frequency of $1,626.2708$ MHz in the L–band.
- Four GPS antennas to record Iridium NEXT signals in the L–band. The antennas feature a multi-point feeding design in order to provide high phase center stability. Also, these wide-beamwidth antennas are designed to receive low elevation signals with high gain. The antennas were arranged in a 4×1 ULA array structure with $d = \lambda = 18.4$ cm. It should be pointed out that ideally the antenna elements should be spaced $d = \frac{\lambda}{2}$ apart to avoid angle ambiguity, however, due to the large diameter of GPS antennas used in this experiment, the antenna spacing was set to λ, which will be discussed in Section IV.2.c.
- A host laptop computer to store the samples of the received signals for off-line post-processing.
  The experimental setup is shown in Figure 1.

It should be noted that DOA estimation is very sensitive to the phase shift between different antenna elements. All antennas, amplifiers, and cables must be similar. Also, all the channels are required to be phase synchronized. To meet these requirements, similar antennas, amplifiers, and matched-length cables were used in this experiment. Moreover, a GPS antenna was used to discipline the USRP's oscillator to maintain the oscillator as stable as possible. However, other elements such as the filters, mixers, amplifiers, and phase locked loops of the USRP can cause a time-varying phase error on the signals received from different antenna elements. Time, temperature, and mechanical conditions are other factors that can introduce a phase error over time. Moreover, mutual coupling between antennas can affect the signals captured by each antenna element. As a result, performing calibration is a crucial step for each experiment to remove the phase and amplitude differences between all the channels with the reference channel.

Figure 1: Experimental hardware setup.

2. Experimental Results

The USRP sampled signals with the sampling bandwidth Fs of 2.4 MHz over a period of about 120 seconds at a carrier frequency of 1626.2708 MHz in the L–band, which coincides with the ring alert (RA) channel of Iridium NEXT SVs. The proposed framework was used to track the Doppler frequency and the azimuth angle of the Iridium NEXT LEO SV with NORAD Catalog Number 42811. It should be noted that since the aim of this paper is to track the azimuth angle and evaluate its effect on positioning accuracy, signals coming from only one Iridium NEXT signal is studied.

a) Acquisition result

As discussed in Section III, in the first step, initial Doppler rate and Doppler are acquired. Figure 2 shows the FFT of the 4th power of the baseband received signal for two successive CPIs, which led to initial Doppler rate estimation. Note that the CPI was set to 2 seconds. After wiping-off the Doppler rate, the FFT of the 4th power of the baseband received signal is taken. The initial Doppler is acquired by normalizing the frequency at which the peak occurs.

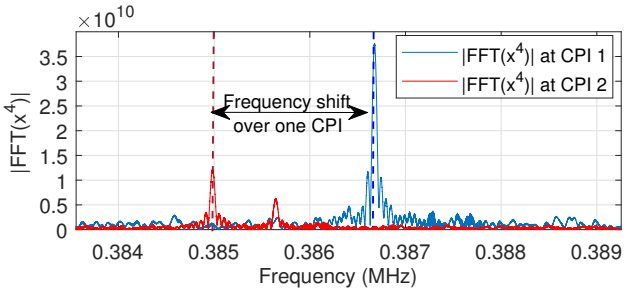

Figure 2: FFT of the 4th power of the received Iridium NEXT signal for two successive CPIs. The frequency shift during a 2-second CPI gives an estimate of $4\beta_0$. Normalizing this value by four gives the initial estimate of the Doppler rate in the acquisition stage.

b) Doppler Tracking Results

In the next step, the Doppler frequency of the signals captured by each antenna element is tracked. The results are compared with the predicted Doppler obtained from two-line element (TLE) files and an SGP4 orbit determination software. Figure 3 demonstrates the estimated (dashed) versus the TLE+SGP4-predicted (solid) Doppler frequency profile for each antenna element. It can be seen that the estimated Doppler frequency matches the predicted Doppler from TLE+SGP4.

c) DOA Tracking Result

In this step, the estimated Doppler frequency is wiped-off from signals received by each antenna element. Collecting the Doppler-compensated samples corresponding to all 4 antennas at each CPI, the sample covariance matrix is calculated to get the MUSIC angular spectrum, as described in Section III.3. Figure 4(a) illustrates the MUSIC angular spectrum over time, where the peaks occur at the estimated azimuth DOA of each CPI. The estimated azimuth angle $\hat{\phi}$ represents the estimated angle between the incoming signal and the orthogonal line to the ULA. Since the array is located along the South-North direction, and the predicted azimuth angle obtained from TLE file, ϕ_{TLE}, is measured from the North direction, the estimated angle and its corresponding azimuth angle from TLE are complementary angles, and they are related through, $\hat{\phi} = 90^\circ - \phi_{TLE} + \alpha_0$, where α_0 represents the initial ambiguity arising from the fact that the distance between the antenna elements equals to λ. This constant ambiguity is resolved in the navigation filter. The estimated angles are disambiguated by comparing them with the azimuth angles from TLE files.

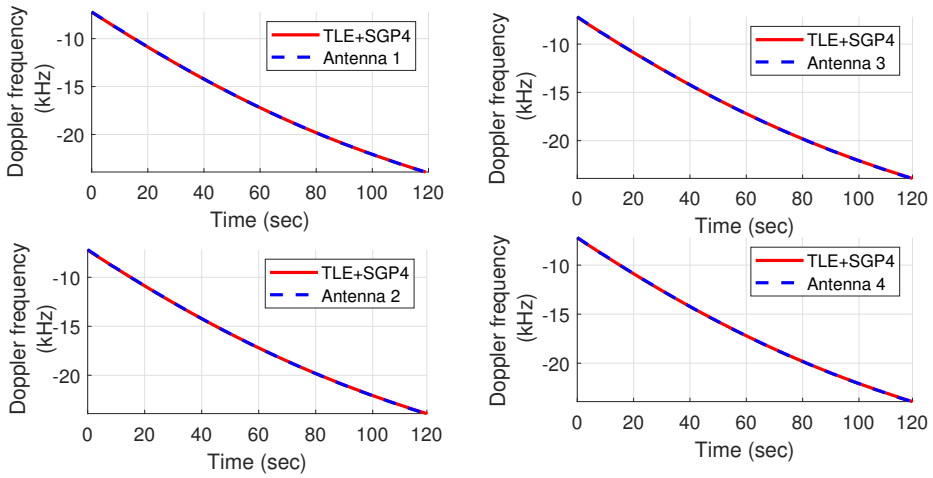

Figure 3: The estimated (dashed) versus the TLE+SGP4-predicted (solid) Doppler frequency profile during the tracking period for all 4 antenna elements.

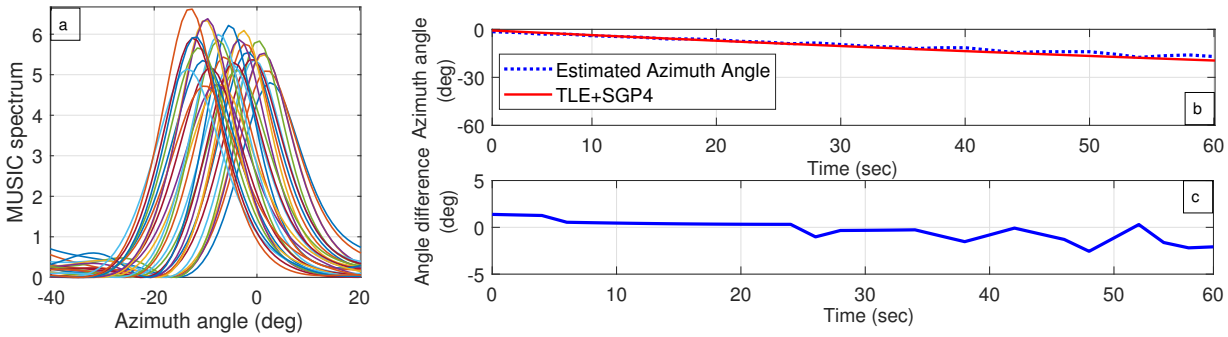

Figure 4: (a) MUSIC angular spectrum of detected Iridium NEXT over time. (b) The estimated (dotted) versus the TLE+SGP4-predicted (solid) azimuth angle profile. (c) Angle estimation error over 60 seconds of Iridium LEO SV visibility.

Figure 4(b) shows the profile of estimated (dotted) versus the TLE+SGP4-predicted (solid) azimuth angle variation. Figure 4(c) demonstrates the error of angle estimation during the tracking period. The experimental results show that the azimuth angles are tracked with an root mean squared-error (RMSE) of 1.04 degrees and with the maximum error of less than 3 degrees during 60 seconds. It can be seen that as the SV approaches the horizon, the angle estimation becomes more erroneous because the received signal power decreases. Antenna element displacements, misalignment of the array due to the slope of the ground, and low number of antenna elements can also contribute in DOA estimation error.

d) Navigation Solution

This section presents positioning results of a stationary receiver with Doppler-only versus Doppler and azimuth DOA measurements produced by the proposed receiver. Pseudorange rate observables $\dot{\rho}$ are formed from the tracked Doppler frequencies according to $\rho = -\frac{c}{f_c} f_D$, where c is the speed of light and $f_c = 1626.2708$ MHz is the carrier frequency. The measurements relating the receiver coordinates to the satellite's estimated pseudorange rate and azimuth DOA from the proposed receiver are modeled as

$$\dot{\rho}(k) = \frac{-\dot{\boldsymbol{r}}_{\mathrm{SV}}^{\top}(k)\left[\boldsymbol{r}_r - \boldsymbol{r}_{\mathrm{SV}}(k)\right]}{\|\boldsymbol{r}_r - \boldsymbol{r}_{\mathrm{SV}}(k)\|} + a_1 + v_{\dot{\rho}}(k) \tag{7}$$

$$\phi(k) = \mathrm{atan2}(y_{r,SV}^{NED}(k),\ x_{r,SV}^{NED}(k)) + a_2 + a_3\, k + v_{\phi}(k), \tag{8}$$

where $\dot{\rho}(k)$ and $\phi(k)$ represent the pseudorange rate and azimuth angle measurements, respectively, at time instant k. $\boldsymbol{r}_{\mathrm{SV}}$ and $\dot{\boldsymbol{r}}_{\mathrm{SV}}$ denote the satellite position and velocity vectors in the Earth-centered Earth-fixed (ECEF) coordinates, with $\boldsymbol{r}_r = [x_r\ y_r\ z_r]^{\top}$ being the receiver position vector; the constant a_1 is assumed to account for the difference between the receiver and the satellite's clocks, i.e., $a_1 = c[\dot{\delta}_r(k) - \dot{\delta}_{SV}(k)]$, where $\dot{\delta}_r$ and $\dot{\delta}_{SV}$ are the receiver's and LEO satellite's clock drifts, respectively; and

$x_{r,SV}^{NED}(k)$ and $y_{r,SV}^{NED}(k)$ are the first and second components of the vector $\boldsymbol{r}_{r,SV}^{NED}(k)$, i.e., the range vector from receiver to satellite in the local North-East-Down (NED) frame,

$$\boldsymbol{r}_{r,SV}^{NED}(k) = \begin{bmatrix} -\sin(\theta_1)\cos(\theta_2) & -\sin(\theta_1)\sin(\theta_2) & \cos(\theta_1) \\ -\sin(\theta_2) & \cos(\theta_2) & 0 \\ -\cos(\theta_1)\cos(\theta_2) & -\cos(\theta_1)\sin(\theta_2) & -\sin(\theta_1) \end{bmatrix} \left[\boldsymbol{r}_{\mathrm{SV}}(k) - \boldsymbol{r}_{\mathrm{r}}(k)\right], \tag{9}$$

Note that, a_2 and a_3 form a time-varying term compensating for unmodeled effects, such as clock errors and ionospheric and tropospheric delays. Moreover, $v_{\dot{\rho}}$ and v_{ϕ} are the measurement noise which are modeled as white Gaussian random variables with variances $\sigma_{\dot{\rho}}^2$ and σ_{ϕ}^2, respectively. Finally, θ_1 and θ_2 are the geodetic latitude and longitude of the unknown receiver defined by $\theta_1 = \arcsin(z_r/\|\boldsymbol{r}_r\|)$ and $\theta_2 = \arctan(y_r/x_r)$. The receiver positioning is achieved via an EKF in two cases of measurement types. First, Doppler measurements are employed to estimate the state vector, $\boldsymbol{x} = \left[\boldsymbol{r}_r^\top, a_1\right]^\top$ with an initial error covariance matrice in the ECEF frame as

$$\mathbf{P}0|0) = \mathrm{diag}[\mathbf{T}\,\mathbf{P}_{NED}(0|0)\,\mathbf{T}^\top, \mathbf{P}_a(0|0)]$$

where $\mathbf{T}$ is the rotation matrix from the NED frame to the ECEF frame, $\mathbf{P}_{NED}(0|0)$ is the initial error covariance matrix in the ECEF frame set to $\mathrm{diag}[6.7\times10^3, 6.7\times10^3, 0.1]$ and $\mathbf{P}_a(0|0)$ is the initial error covariance corresponding to a_1 and is set to 10^4. Afterward, the azimuth measurements are added to the Doppler to solve the positioning problem. In this case, the state vector is augmented to $\boldsymbol{x} = \left[\boldsymbol{r}_r^\top, a_1, a_2, a_3\right]^\top$, where $\mathbf{P}_{NED}(0|0)$ remains the same while $\mathbf{P}_a(0|0)$ is changed to $[10^4, 10^4, 10^4]$. The measurement noise variances for Doppler and azimuth where calculated empirically and ranged between $1-25$ Hz^2 and $0.25-2.25$ deg^2, respectively. Figure 5 summarizes the positioning results, which demonstrates the benefit of fusing azimuth DOA alongside Doppler measurements.

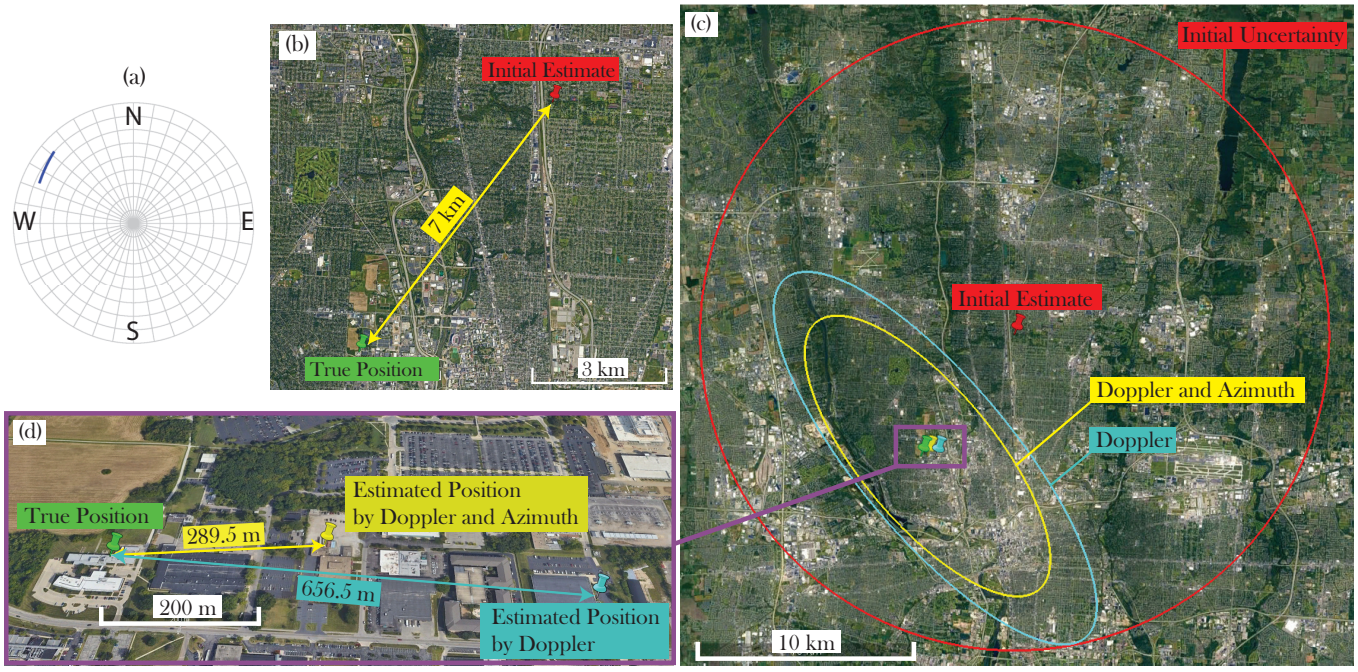

Figure 5: (a) Skyplot showing the trajectory of the Iridium LEO satellite. (b) Initial estimate versus true receiver position. (c) Initial estimate and its corresponding 95% uncertainty ellipses and estimated position with (i) Doppler-only measurements and (ii) Doppler and azimuth DOA along with corresponding 95% uncertainty ellipses. (d) Zoomed view on positioning errors. Map data: Google Earth.

V. CONCLUSION

This paper presented a receiver for Doppler and Azimuth DOA estimation of Iridium NEXT LEO satellite signals. Experimental results were presented demonstrating successful tracking of the Doppler frequency and azimuth DOA of an Iridium NEXT LEO satellite, achieving a Doppler RMSE of 8.1 Hz over 120 seconds and an azimuth DOA RMSE of 1.04 degrees over 60 seconds. The Doppler and azimuth DOA measurements are fused via an EKF to localize a stationary receiver. Starting with an initial estimate 7 km away from the true receiver's position, Doppler-only measurements yielded a final positioning error of 656.m, while the Doppler and azimuth DOA measurements reduced the error to 289.5 m.

ACKNOWLEDGEMENTS

This work was supported in part by the Office of Naval Research (ONR) under Grant N00014-19-1-2511 and in part by the Air Force Office of Scientific Research (AFOSR) under Grant FA9550-22-1-0476. The authors would like to thank Justin Kuric for helpful discussions.

REFERENCES

Abu-Shaban, Z., Zhou, X., Abhayapala, T., Seco-Granados, G., and Wymeersch, H. (2018). Error bounds for uplink and downlink 3D localization in 5G millimeter wave systems. *IEEE Transactions on Wireless Communications*, 17(8):4939–4954.

Aziz, M. and Allen, C. (2018). Experimental results of a differential angle-of-arrival based 2D localization method using signals of opportunity. *International Journal of Navigation and Observation*, 2018(5470895):1–6.

Benzerrouk, H., Nguyen, Q., Xiaoxing, F., Amrhar, A., Nebylov, A., and Landry, R. (2019). Alternative PNT based on Iridium Next LEO satellites Doppler/INS integrated navigation system. In *Proceedings of Saint Petersburg International Conference on Integrated Navigation Systems*, pages 1–10.

Chen, X., Wei, Q., Wang, F., Jun, Z., Wu, S., and Men, A. (2020). Super-resolution time of arrival estimation for a symbiotic FM radio data system. *IEEE Transactions on Broadcasting*, 66(4):847–856.

Clerckx, B. and Oestges, C. (2013). *MIMO Wireless Networks: Channels, Techniques and Standards for Multi-Antenna, Multi-User and Multi-Cell Systems*. Academic Press, Inc., Orlando, FL, USA, 2nd edition.

Farhangian, F., Benzerrouk, H., and Landry, R. (2021). Opportunistic in-flight INS alignment using LEO satellites and a rotatory IMU platform. *Aerospace*, 8(10):280–281.

Farhangian, F. and Landry, R. (2020). Multi-constellation software-defined receiver for Doppler positioning with LEO satellites. *Sensors*, 20(20):5866–5883.

Fascista, A., Coluccia, A., Wymeersch, H., and Seco-Granados, G. (2019). Millimeter-wave downlink positioning with a single-antenna receiver. *IEEE Transactions on Wireless Communications*, 18(9):4479–4490.

Fokin, G. and Volgushev, D. (2022). Software-defined radio network positioning technology design. problem statement. In *Proceedings of Systems of Signals Generating and Processing in the Field of on Board Communications*, pages 1–6.

Gao, Y., Zhao, X., Wang, S., Xiang, Y., Huang, C., and Hua, Y. (2021). Positioning via GEO communication satellites' signals of opportunity. *IET Radar, Sonar Navigation*, 15(11):1472–1482.

Hartnett, M. (2022). Performance assessment of navigation using carrier Doppler measurements from multiple LEO constellations. Master's thesis, Air Force Institute of Technology, Ohio, USA.

Hong, T., Sun, J., Jin, T., Yi, Y., and Qu, J. (2021). Hybrid positioning with DTMB and LTE signals. In *Proceedings of International Wireless Communications and Mobile Computing*, pages 303–307.

Huang, C., Qin, H., Zhao, C., and Liang, H. (2022). Phase - time method: Accurate Doppler measurement for Iridium NEXT signals. *IEEE Transactions on Aerospace and Electronic Systems*, 58(6):5954–5962.

Iridium Constellation LLC (2013). Iridium NEXT engineering statement. `http://licensing.fcc.gov/myibfs/download.do?attachment_key=1031348`.

Islam, M., Wang, T., Wade, S., Bessell, T., Spitzer, T., and Hallett, J. (2021). Doppler and angle of arrival estimation from digitally modulated satellite signals in passive RF space domain awareness. In *Proceedings of Advanced Maui Optical and Space Surveillance Technologies Conference*, pages 1–14.

Jardak, N. and Jault, Q. (2022). The potential of LEO satellite-based opportunistic navigation for high dynamic applications. *Sensors*, 22(7):2541–2565.

Jiao, Z., Chen, L., Lu, X., Liu, Z., Zhou, X., Zhuang, Y., and Guo, G. (2023). Carrier phase ranging with DTMB signals for urban pedestrian localization and GNSS aiding. *Remote Sensing*, 15(2):423–446.

Kassas, Z. and Abdallah, A. (2023). No GPS no problem: Exploiting cellular OFDM-based signals for accurate navigation. *IEEE Transactions on Aerospace and Electronic Systems*. accepted.

Kassas, Z., Khairallah, N., and Kozhaya, S. (2023a). Ad astra: Simultaneous tracking and navigation with megaconstellation LEO satellites. *IEEE Aerospace and Electronic Systems Magazine*. accepted.

Kassas, Z., Khalife, J., Abdallah, A., and Lee, C. (2022). I am not afraid of the GPS jammer: resilient navigation via signals of opportunity in GPS-denied environments. *IEEE Aerospace and Electronic Systems Magazine*, 37(7):4–19.

Kassas, Z., Kozhaya, S., Kanj, H., Saroufim, J., Hayek, S., Neinavaie, M., Khairallah, N., and Khalife, J. (2023b). Navigation with multi-constellation LEO satellite signals of opportunity: Starlink, Oneweb, Orbcomm, and Iridium. In *Proceedings of IEEE/ION Position, Location, and Navigation Symposium*, pages 338–343.

Kassas, Z., Neinavaie, M., Khalife, J., Khairallah, N., Haidar-Ahmad, J., Kozhaya, S., and Shadram, Z. (2021). Enter LEO on the GNSS stage: Navigation with Starlink satellites. *Inside GNSS Magazine*, 16(6):42–51.

Khalife, J. and Kassas, Z. (2019). Receiver design for Doppler positioning with LEO satellites. In *Proceedings of IEEE International Conference on Acoustics, Speech and Signal Processing*, pages 5506–5510.

Khalife, J. and Kassas, Z. (2023). Differential framework for submeter-accurate vehicular navigation with cellular signals. *IEEE Transactions on Intelligent Vehicles*, 8(1):732–744.

Khalife, J., Neinavaie, M., and Kassas, Z. (2020). Navigation with differential carrier phase measurements from megaconstellation LEO satellites. In *Proceedings of IEEE/ION Position, Location, and Navigation Symposium*, pages 1393–1404.

Khalife, J., Neinavaie, M., and Kassas, Z. (2022). The first carrier phase tracking and positioning results with Starlink LEO satellite signals. *IEEE Transactions on Aerospace and Electronic Systems*, 56(2):1487–1491.

Kozhaya, S., Kanj, H., and Kassas, Z. (2023). Multi-constellation blind beacon estimation, Doppler tracking, and opportunistic positioning with OneWeb, Starlink, Iridium NEXT, and Orbcomm LEO satellites. In *Proceedings of IEEE/ION Position, Location, and Navigation Symposium*, pages 1184–1195.

Kozhaya, S. and Kassas, Z. (2022). Blind receiver for LEO beacon estimation with application to UAV carrier phase differential navigation. In *Proceedings of ION GNSS Conference*, pages 2385–2397.

Lapin, I., Granados, G., Samson, J., Renaudin, O., Zanier, F., and Ries, L. (2022). STARE: Real-time software receiver for LTE and 5G NR positioning and signal monitoring. In *Proceedings of Workshop on Satellite Navigation Technology*, pages 1–11.

Lee, J., Gil, G., and Lee, Y. (2014). Exploiting spatial sparsity for estimating channels of hybrid MIMO systems in millimeter wave communications. In *Proceedings of IEEE GLOBECOM*, pages 3326–3331.

Leng, M., Quitin, F., Tay, W., Cheng, C., Razul, S., and See, C. (2016). Anchor-aided joint localization and synchronization using SOOP: Theory and experiments. *IEEE Transactions on Wireless Communications*, 15(11):7670–7685.

Liu, Z., Chen, L., Zhou, X., Jiao, Z., Guo, G., and Chen, R. (2023). Machine learning for time-of-arrival estimation with 5G signals in indoor positioning. *IEEE Internet of Things Journal*, 10(11):9782–9795.

Ma, W., Qi, C., and Li, G. (2020). High-resolution channel estimation for frequency-selective mmwave massive MIMO systems. *IEEE Transactions on Wireless Communications*, 19(5):3517–3529.

Maaref, M. and Kassas, Z. (2022). Autonomous integrity monitoring for vehicular navigation with cellular signals of opportunity and an IMU. *IEEE Transactions on Intelligent Transportation Systems*, 23(6):5586–5601.

Mendrzik, R., Wymeersch, H., and Bauch, G. (2018). Joint localization and mapping through millimeter wave MIMO in 5G systems. In *Proceedings of IEEE Global Communications Conference*, pages 1–6.

Moghtadaiee, V. and Dempster, A. (2014). Indoor location fingerprinting using FM radio signals. *IEEE Transactions on Broadcasting*, 60(2):336–346.

Orabi, M., Khalife, J., and Kassas, Z. (2021). Opportunistic navigation with Doppler measurements from Iridium Next and Orbcomm LEO satellites. In *Proceedings of IEEE Aerospace Conference*, pages 1–9.

Pan, M., Liu, P., Liu, S., Qi, W., Huang, Y., You, X., Jia, X., and Li, X. (2022). Efficient joint DOA and TOA estimation for indoor positioning with 5G picocell base stations. *IEEE Transactions on Instrumentation and Measurement*, 71:1–19.

Paulraj, A., Ottersten, B., Roy, R., Swindlehurst, A., Xu, G., and Kailath, T. (1993). 16 subspace methods for directions-of-arrival estimation. *Handbook of Statistics*, 10:693–739.

Prol, F., Ferre, R., Saleem, Z., Välisuo, P., Pinell, C., Lohan, E., Elsanhoury, M., Elmusrati, M., Islam, S., Celikbilek, K., Selvan, K., Yliaho, J., Rutledge, K., Ojala, A., Ferranti, L., Praks, J., Bhuiyan, M., Kaasalainen, S., and Kuusniemi, H. (2022). Position, navigation, and timing (PNT) through low earth orbit (LEO) satellites: A survey on current status, challenges, and opportunities. *IEEE Access*, 10:83971–84002.

Psiaki, M. (2021). Navigation using carrier Doppler shift from a LEO constellation: TRANSIT on steroids. *NAVIGATION, Journal of the Institute of Navigation*, 68(3):621–641.

Psiaki, M. and Slosman, B. (2019). Tracking of digital FM OFDM signals for the determination of navigation observables. In *Proceedings of ION GNSS Conference*, pages 2325–2348.

Raquet *et al.*, J. (2021). Position, navigation, and timing technologies in the 21st century. volume 2, Part D: Position, Navigation, and Timing Using Radio Signals-of-Opportunity, chapter 35–43, pages 1115–1412. Wiley-IEEE.

Rastorgueva-Foi, E., Costa, M., Koivisto, M., Leppanen, K., and Valkama, M. (2018). User positioning in mmw 5G networks using beam-RSRP measurements and Kalman filtering. In *Proceedings of International Conference on Information Fusion*, pages 1–7.

Shahriar, C. (2008). A scheme to mitigate interference from Iridium satellite's downlink signal captured by omnidirectional antenna array. In *Proceedings of IEEE Antennas and Propagation Society International Symposium*, pages 1–4.

Shamaei, K. and Kassas, Z. (2021a). A joint TOA and DOA acquisition and tracking approach for positioning with LTE signals. *IEEE Transactions on Signal Processing*, 69:2689–2705.

Shamaei, K. and Kassas, Z. (2021b). Receiver design and time of arrival estimation for opportunistic localization with 5G signals. *IEEE Transactions on Wireless Communications*, 20(7):4716–4731.

Shamaei, K., Khalife, J., and Kassas, Z. (2018). A joint TOA and DOA approach for positioning with LTE signals. In *Proceedings of IEEE/ION Position, Location, and Navigation Symposium*, pages 81–91.

Shi, C., Zhang, Y., and Li, Z. (2023). Revisiting Doppler positioning performance with LEO satellites. *GPS Solutions*, 27(3):126–137.

Soderini, A., Thevenon, P., Macabiau, C., Borgagni, L., and Fischer, J. (2020). Pseudorange measurements with LTE physical channels. In *Proceedings of ION International Technical Meeting*, pages 817–829.

Souli, N., Kolios, P., and Ellinas, G. (2022). Online relative positioning of autonomous vehicles using signals of opportunity. *IEEE Transactions on Intelligent Vehicles*, 7(4):873–885.

Souli, N., Makrigiorgis, R., Kolios, P., and Ellinas, G. (2021). Real-time relative positioning system implementation employing signals of opportunity, inertial, and optical flow modalities. In *Proceedings of International Conference on Unmanned Aircraft Systems*, pages 229–236.

Tan, Z., Qin, H., Cong, L., and Zhao, C. (2019a). New method for positioning using IRIDIUM satellite signals of opportunity. *IEEE Access*, 7:83412–83423.

Tan, Z., Qin, H., Cong, L., and Zhao, C. (2019b). Positioning using IRIDIUM satellite signals of opportunity in weak signal environment. *Electronics*, 9(1):37.

Thompson, S., Martin, S., and Bevly, D. (2021). Single differenced Doppler positioning with low Earth orbit signals of opportunity and angle of arrival estimation. In *Proceedings of ION International Technical Meeting Conference*, pages 497–509.

Tian, J., Fangchi, L., Yafei, T., and Dongmei, L. (2023). Utilization of non-coherent accumulation for LTE TOA estimation in weak LOS signal environments. *EURASIP Journal on Wireless Communications and Networking*, 2023(1):1–31.

Wang, P. and Morton, Y. (2023). Impact analysis of inter-cell interference in cellular networks for navigation applications. *IEEE Transactions on Aerospace and Electronic Systems*, 59(1):685–694.

Wei, Q., Chen, X., and Zhan, Y. (2020). Exploring implicit pilots for precise estimation of LEO satellite downlink Doppler frequency. *IEEE Communications Letters*, 24(10):2270–2274.

Yang, C., Arizabaleta-Diez, M., Weitkemper, P., and Pany, T. (2022). An experimental analysis of cyclic and reference signals of 4G LTE for TOA estimation and positioning in mobile fading environments. *IEEE Aerospace and Electronic Systems Magazine*, 37(9):16–41.

Yang, C. and Soloviev, A. (2020). Mobile positioning with signals of opportunity in urban and urban canyon environments. In *Proceedings of IEEE/ION Position, Location, and Navigation Symposium*, pages 1043–1059.

Zhao, C., Qin, H., Wu, N., and Wang, D. (2023). Analysis of baseline impact on differential doppler positioning and performance improvement method for LEO opportunistic navigation. *IEEE Transactions on Instrumentation and Measurement*, 72:1–10.